



City Research Online

City, University of London Institutional Repository

Citation: Dissanayake, D. M. M. P., Poologanathan, K., Gunalan, S., Tsavdaridis, K. D., Nagaratnam, B. & Wanniarachchi, K. (2020). Numerical modelling and shear design rules of stainless steel lipped channel sections. *Journal of Constructional Steel Research*, 168, doi: 10.1016/j.jcsr.2019.105873

This is the accepted version of the paper.

This version of the publication may differ from the final published version.

Permanent repository link: <https://openaccess.city.ac.uk/id/eprint/27023/>

Link to published version: <https://doi.org/10.1016/j.jcsr.2019.105873>

Copyright: City Research Online aims to make research outputs of City, University of London available to a wider audience. Copyright and Moral Rights remain with the author(s) and/or copyright holders. URLs from City Research Online may be freely distributed and linked to.

Reuse: Copies of full items can be used for personal research or study, educational, or not-for-profit purposes without prior permission or charge. Provided that the authors, title and full bibliographic details are credited, a hyperlink and/or URL is given for the original metadata page and the content is not changed in any way.



City Research Online

City, University of London Institutional Repository

Citation: Dissanayake, DMMP, Poologanathan, K, Gunalan, S, Tsavdaridis, KD ORCID: 0000-0001-8349-3979, Nagaratnam, B and Wanniarachchi, KS (2020). Numerical modelling and shear design rules of stainless steel lipped channel sections. Journal of Constructional Steel Research, 168, doi: 10.1016/j.jcsr.2019.105873

This is the draft version of the paper.

This version of the publication may differ from the final published version.

Permanent repository link: <https://openaccess.city.ac.uk/id/eprint/27023/>

Link to published version: <http://dx.doi.org/10.1016/j.jcsr.2019.105873>

Copyright: City Research Online aims to make research outputs of City, University of London available to a wider audience. Copyright and Moral Rights remain with the author(s) and/or copyright holders. URLs from City Research Online may be freely distributed and linked to.

Reuse: Copies of full items can be used for personal research or study, educational, or not-for-profit purposes without prior permission or charge. Provided that the authors, title and full bibliographic details are credited, a hyperlink and/or URL is given for the original metadata page and the content is not changed in any way.

Numerical Modelling and Shear Design Rules of Stainless Steel Lipped Channel Sections

D. M. M. P. Dissanayake

Faculty of Engineering and Environment, University of Northumbria,
Newcastle, UK.

K. Poologanathan

Faculty of Engineering and Environment, University of Northumbria,
Newcastle, UK.

S. Gunalan

School of Engineering and Built Environment, Griffith University,
Gold Coast, Australia.

K. D. Tsavdaridis

School of Civil Engineering, University of Leeds, UK.

B. Nagaratnam

Faculty of Engineering and Environment, University of Northumbria,
Newcastle, UK.

K. S. Wanniarachchi

Faculty of Engineering, University of Ruhuna, Sri Lanka.

Abstract

The demand for highly structurally efficient stainless steel is limited to a certain extent by its high initial cost. Therefore, the utilisation of material to the optimum possible level is important. In achieving this, further consideration should be given to enhance the design rules where beneficial effects such as pronounced strain hardening in stainless steel should be taken into account in the design process. In addition to that, a thorough understanding of the structural behaviour of stainless steel sections is also required. However, the shear behaviour and capacity of cold-formed stainless steel lipped channel beams (LCBs) have not been thoroughly investigated previously. Therefore, experimental and detailed finite element (FE) modelling were undertaken to investigate the shear behaviour and strength of stainless steel LCBs. A comprehensive parametric study was also conducted by developing 100 FE models. From the results, the available post-buckling strength in slender stainless steel LCBs was highlighted.

Furthermore, the beneficial strength increment due to the strain hardening effect of stainless steel, particularly for compact LCBs in shear, was investigated. Comparisons indicated that current EN1993-1-4 and direct strength method (DSM) shear design rules are too conservative in particular for compact sections. Thus, existing shear design rules were modified to enhance the overall prediction accuracy for stainless steel LCBs while attention was given to capture the available inelastic reserve capacity.

Keywords: Cold-formed stainless steel; Lipped channel beams; Finite element modelling; Shear design rules; EN1993-1-4; Direct strength method

1 Introduction

Stainless steel is becoming a highly demanding construction material (see Figure 1 for application of stainless steel in structures [1]). This is primarily due to its improved characteristics as a result of the well-controlled alloying composition of each stainless steel grade. Thus stainless steel usually exhibits appealing characteristics such as higher strength-to-weight ratio, high ductility, impact resistance, fire resistance and good corrosion resistance thus featuring greater durability and low maintenance cost, and also recyclability in addition to its aesthetically pleasing good finish. The chromium content of stainless steel is more than 10.5 % and it contributes to form a chromium-rich oxide layer on the surface of stainless steel [2]. This is the main reason for its high corrosion resistance. However, these benefits have come to a cost due to the alloying composition (chromium and nickel) of stainless steel, thus, the material usage should be optimised by giving more attention to the design process of stainless steel structural members.



Figure 1: Gent Sint Pieters railway station, Belgium [1].

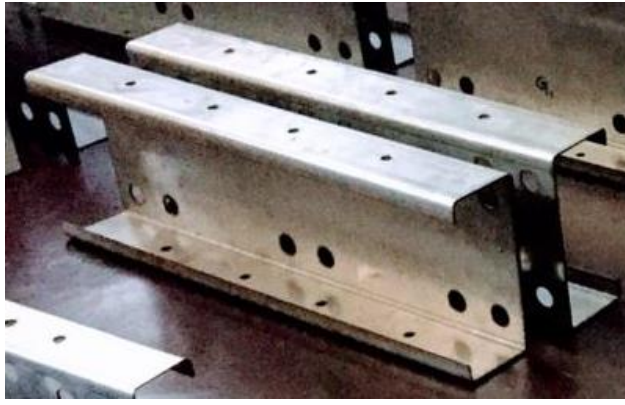
Over the past few years, research into stainless steel sections has covered numerous cross-section types. Available stub column tests of square, rectangular and circular hollow sections, I-sections, angle sections, and channel sections have been gathered and reported alongside with bending tests of the above mentioned hollow sections and I-sections by Gardner and Theofanous [3]. Channels under minor axis bending have been studied by Theofanous et al. [4] while channels under combined loading have been investigated by Liang et al. [5,6]. Furthermore, angles, channels and T-sections in bending about an axis that is not symmetry have been covered by Zhao and Gardner [7]. Moreover, distortional-global interaction buckling of stainless steel lipped channel sections have been investigated in [8,9] while a recent research provides the details of major axis bending behaviour of lipped channel sections [10]. In addition, previous studies have been conducted on the shear behaviour of cold-formed steel channel sections by Keerthan and Mahendran [11–13]. Furthermore, studies have been conducted on the combined bending and shear behaviour of high strength cold-formed steel C-sections and purlins by Pham and Hancock [14,15]. However, it is worth to note that there is no comprehensive study available for shear behaviour of stainless steel lipped channel sections.

Currently, available design guidelines for stainless steel sections include European codes such as EN1993-1-4 [16] and EN1993-1-5 [17], Australian/New Zealand standard AS/NZS 4673 [18], and American specification SEI/ASCE-8 [19]. These design guidelines are in accordance with the conventional carbon steel design guidelines, thus utilise the elastic, perfectly-plastic material models [20] limiting the ultimate strength to yield stress of the material, which is not true for stainless steel as it shows a non-linear stress-strain behaviour due to its pronounced strain hardening effect. In addition, these design guidelines are based on the conventional cross-section classification approach, known as the effective width method, which considers cross sections as an assemblage of plate elements [21]. However, it has been proved that there is a considerable post-buckling strength in channel sections due to the element interaction presented at the web-flange juncture [13]. Therefore, the main concern in the design process should be given to the pronounced strain hardening effect of stainless steel which emphasises the continuation of strength beyond yield stress, and to the requirement of accounting for element interaction. In order to address these shortcomings in the current design guidelines, advanced design approaches, such as the continuous strength method (CSM) and the direct strength method (DSM), have been proposed.

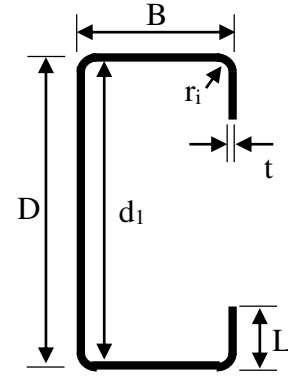
In this paper, the shear behaviour of stainless steel LCBs is investigated with scope to improve the shear capacity prediction accuracy using EN1993-1-4 [16] and DSM. The application of CSM to predict the shear capacity of stainless steel LCBs is not investigated herein, thus recommended as future work. Conducted experiments were utilised to develop accurate and reliable finite element (FE) models of stainless steel LCBs, details of which are elaborated in the paper. In order to collect a comprehensive database on the shear behaviour of stainless steel LCBs, a detailed parametric study was conducted following the validation of the FE models. Common austenitic and duplex stainless steel grades and both compact and slender cross sections were considered. Improved shear design equations are presented while confirming their prediction accuracy. Moreover, pronounced inelastic reserve capacity in compact stainless steel LCBs is highlighted and attempts were made to capture this in capacity prediction equations.

2 Experimental study

To study the shear behaviour of stainless steel LCBs a testing programme was conducted. The testing programme was comprised of nine cold-formed stainless steel lipped channel sections made of austenitic stainless steel grade 1.4301. Three sectional geometries (with section depths of 100 mm, 150 mm and 200 mm) with three different section thicknesses (1.2 mm, 1.5 mm and 2.0 mm) were chosen to represent a range of slenderness values. Figure 2 shows the tested stainless steel lipped channel sections and the notations used for the cross-sectional dimensions where D is the section depth, B is the width of the flange, L is the depth of the lip, d_1 is the clear web depth, t is the thickness and r_1 is the internal corner radius. All LCB cross sections are denoted as LCB $D \times B \times L \times t$ where LCB stands for Lipped Channel Beam followed by the nominal section dimensions in millimetres (section depth $D \times$ flange width $B \times$ lip depth $L \times$ section thickness t). Table 1 provides the measured cross sectional dimensions of the stainless steel LCBs employed in the experimental programme.



(a)



(b)

Figure 2: (a) Tested stainless steel lipped channel sections; (b) Cross section details.

Table 1: Dimensions of the tested stainless steel LCBs.

<i>Section</i>	d_1 (mm)	B (mm)	L (mm)	t (mm)	r_i (mm)
LCB 100×50×15×1.2	97.5	50	16.5	1.18	2.0
LCB 100×50×15×1.5	97	50.25	16.25	1.5	2.0
LCB 100×50×15×2.0	95.5	50.25	16.5	1.99	2.0
LCB 150×65×15×1.2	147	65.5	16	1.18	2.0
LCB 150×65×15×1.5	147	66	16.5	1.5	2.0
LCB 150×65×15×2.0	146.5	65.5	16	1.99	2.0
LCB 200×75×15×1.2	197	75.5	16.25	1.18	2.0
LCB 200×75×15×1.5	198	76.75	15	1.5	2.0
LCB 200×75×15×2.0	197	75.5	15.5	1.99	2.0

To obtain the mechanical properties of the used stainless steel grade, tensile coupon tests were conducted. Coupons were extracted from the middle part of the web and flanges of the sections covering all the sections used here. Coupons were tested at a uniform strain rate of 0.0005 s^{-1} . Obtained mechanical properties were utilised in the development of the finite element models to validate the experiments. Average values of Young's modulus (E), 0.01% proof stress ($\sigma_{0.01}$), 0.2% proof stress ($\sigma_{0.2}$), ultimate tensile stress (σ_u), Ramberg-Osgood parameters n and m , strain corresponding to the ultimate tensile stress (ϵ_u) and strain at fracture (ϵ_f) are listed in Table 2.

Table 2: Average material properties of the stainless steel grade 1.4301 extracted from tensile coupon test.

	E	$\sigma_{0.01}$	$\sigma_{0.2}$	σ_u	n	m	ε_u	ε_f
	(GPa)	(MPa)	(MPa)	(MPa)				
Average value	197.3	161.2	253.9	725.3	6.6	1.98	0.54	0.61

LCB is a mono-symmetric open section thus an unbalanced shear flow presents within its cross section. Therefore, in the experimental setup back-to-back LCBs were used in order to eliminate any torsional effects. Two LCBs were attached together back-to-back using three T-shaped stiffeners in between them at the two ends and at the mid-span. All the specimens were subjected to three-point loading configuration by applying a point load at the mid-span of the simply supported back-to-back beam setup. Figure 3 illustrates the three-point loading arrangement while Figure 4 shows the back-to-back LCBs setup used in the testing.

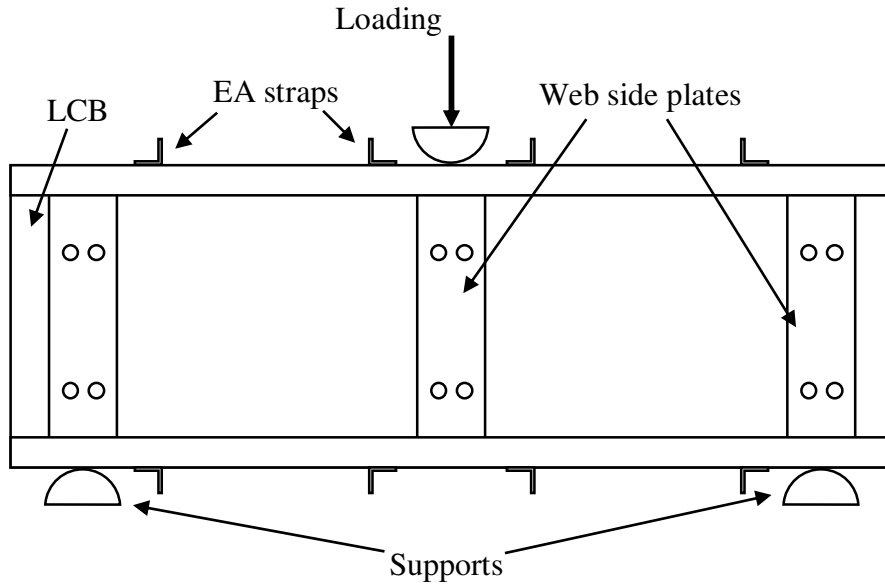


Figure 3: Schematic diagram of three-point loading arrangement.

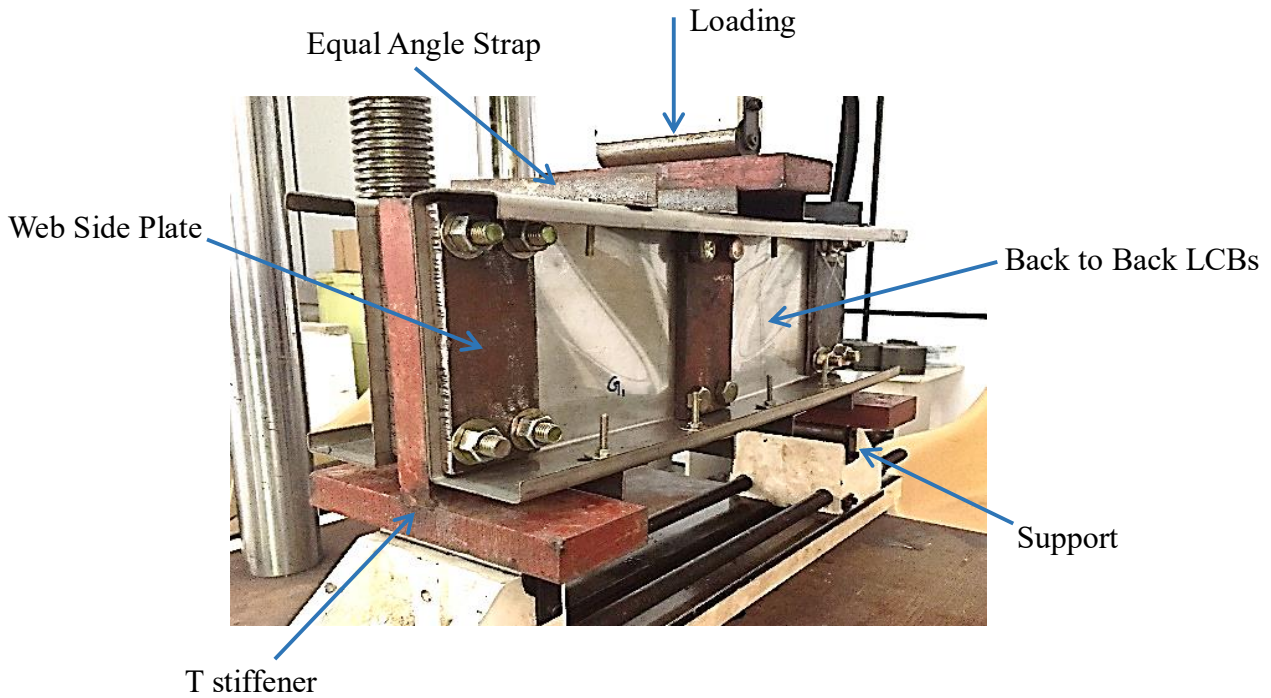


Figure 4: Experimental setup.

Displacement control was employed in the loading head with a constant downward moving rate of 0.7 mm/min. At the mid-span, loading head was attached to the T-stiffener. Then the load was transferred to two specimens. 10 mm thick full depth rigid plates were attached to the specimen webs at the mid-span and at the two ends to avoid any web bearing failure. At the beam ends, a pin and a roller support were assigned to the T-stiffeners to simulate simply supported conditions. A 30 mm gap was maintained between two LCBs in the back-to-back setup using T-stiffeners. Due to this, two LCBs were able to behave independently while remaining as one unit to resist torsional effects. Spacing between two vertical rows of bolts at each rigid plate was 45 mm. At the supports, a 25 mm overhang was kept to the beam edge from the outer bolt row.

Equal angle straps were attached to the both top and bottom flanges adjacent to the supports and to the loading point. The purpose of this straps were to prevent any distortional buckling that the sections could undergo. Keerthan and Mahendran [12] showed that the shear capacity of a section is not affected by the bending stresses for sections with shorter spans (with an aspect ratio=1.0) while combined bending and shear interaction should be considered for sections with relatively longer spans. Therefore, all the LCBs employed in the testing programme had relatively shorter spans with an aspect ratio (shear span (a)/ clear web depth

(d_1) of 1.0 in order to govern the shear failure mode and to suppress the bending failure mode. Vertical displacements of the LCBs were measured at the mid-span by using two Linear Variable Differential Transducers (LVDTs).

Table 3: Ultimate loads and shear capacities obtained from experiments for stainless steel sections.

<i>Section</i>	P_T (kN)	$V_T = P_T / 4$ (kN)
LCB 100×50×15×1.2	74.0	18.5
LCB 100×50×15×1.5	97.8	24.4
LCB 100×50×15×2.0	144.0	36.0
LCB 150×65×15×1.2	86.4	21.6
LCB 150×65×15×1.5	105.1	26.3
LCB 150×65×15×2.0	174.2	43.6
LCB 200×75×15×1.2	91.9	23.0
LCB 200×75×15×1.5	105.9	-
LCB 200×75×15×2.0	188.2	47.1

Table 3 summarises the ultimate peak loads (P_T) recorded in the experiments for all the nine LCBs with the calculated ultimate shear capacities (V_T). For LCB 200×75×15×1.5 specimen, premature failure was observed during the test as the bolts at the loading point were failed due to the yielding. Therefore, this test result was not considered in the validation process and excluded from the design calculations. All the tests conducted exhibited shear failure modes as expected and shear failure modes of LCB 150×65×15×2 and LCB 200×75×15×1.2 specimens are illustrated in Figure 5. Load-deflection curve for LCB 150×65×15×2.0 section is shown in Figure 6 as recorded during the testing programme.

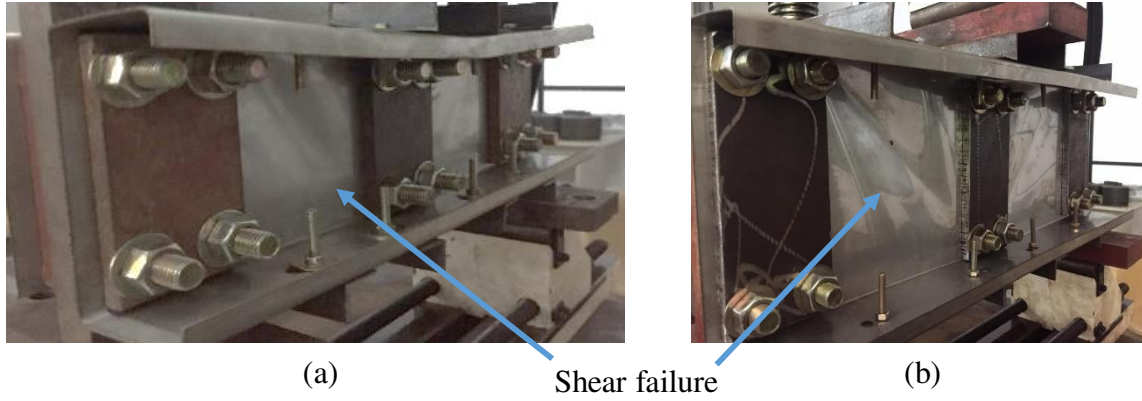


Figure 5: Shear failure modes (a) LCB 150×65×15×2; (b) LCB 200×75×15×1.2.

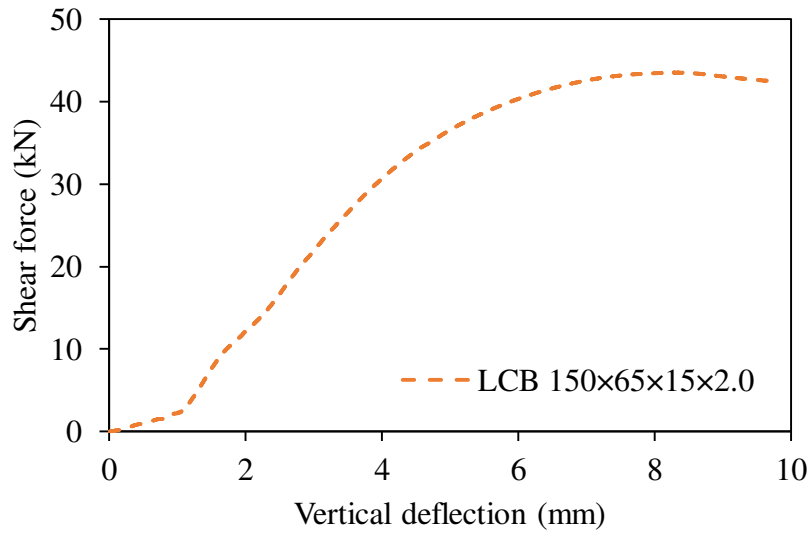


Figure 6: Load-deflection curve of LCB 150×65×15×2.0 section.

3 Finite Element (FE) modelling

3.1 General

This section provides the details of the development of FE models which were then used to investigate the shear behaviour of LCBs. A detailed parametric study was conducted using the developed FE models following the validation process, details of which are presented in the next section. For the validation of the FE models, experimental results of both stainless steel and cold-formed steel sections were employed. The details of cold-formed steel sections employed in the validation process can be found from Keerthan and Mahendran [12]. For the

development of the FE models, the commercially available FE software package ABAQUS CAE 2017 was used.

When developing FE models single LCBs were employed considering the symmetry of the test setup instead of the back-to-back setup, in order to reduce the computational cost associated with simulation running time. Appropriate boundary conditions were introduced to simulate real conditions and LCBs were supported and loaded through the shear centre using single web side plates to reduce torsional effects. The contact between the web side plate and the LCB web was defined as tie constraints available in Abaqus. The shear centre location was calculated using THIN-WALL-2 [22] software. Similar FE models were employed previously [23], and deemed to provide good accuracy with test results.

3.2 Element type and FE mesh

S4R shell elements available in Abaqus were employed in the FE models as they account for finite membrane strains and large rotations, thus allowing for large-strain analysis [24]. S4R shell element type has four nodes and six degrees of freedom per each node. The successful use of S4R shell elements in thin-walled sections subject to shear has been previously proven by Sonu and Singh [25]. By conducting a mesh sensitivity analysis, it was found that 5 mm × 5 mm sized mesh was able to provide convergence with reasonably good accuracy. However, for the corners relatively smaller mesh of 1 mm was employed in the transverse direction to define the curvature. Relatively larger mesh was employed for the web side plates since more focus has been given to the LCB section behaviour, thus allowing more efficient simulation time. Figure 7 shows the FE mesh of the LCB section and web side plates.

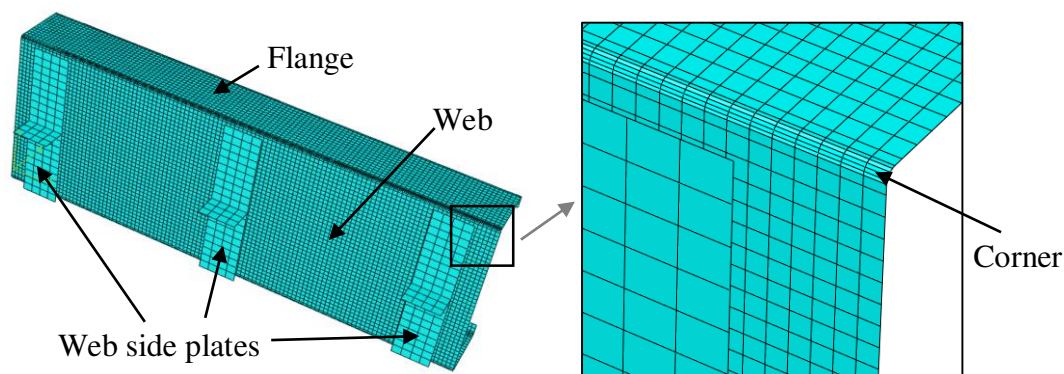


Figure 7: FE mesh of LCB and web side plates.

3.3 Material model

Stainless steel exhibits non-linear stress-strain behaviour due to its pronounced strain hardening effect. Over the past years, numerous material models have been proposed to accurately capture this non-linear behaviour. Recently, the existing two-stage Ramberg-Osgood material model has been modified by Arrayago et al. [26] and the proposals are recommended to be included in future revisions of EN1993-1-4 [16]. Therefore to define the stress-strain relationship of stainless steel, modified two-stage Ramberg-Osgood material model proposed by Arrayago et al. [26] was used. Then true stress (σ_{true}) and log plastic strain (ε_{ln}^{pl}) were calculated using Eqs. (1) and (2) and incorporated into Abaqus as a multilinear curve with sufficient points to represent the accurate stress-strain behaviour. It is worth to note that for the developed cold-formed steel FE models, elastic, perfectly-plastic material model was incorporated.

$$\sigma_{true} = \sigma_{nom}(1 + \varepsilon_{nom}) \quad (1)$$

$$\varepsilon_{ln}^{pl} = \ln(1 + \varepsilon_{nom}) - \frac{\sigma_{true}}{E} \quad (2)$$

where σ_{nom} and ε_{nom} are engineering stress and strain, respectively.

3.4 Corner strength enhancement and residual stresses

During the cold-forming process of LCBs corner regions undergo larger plastic deformations. This results in considerable increase in material strength particularly in stainless steel which is termed as cold-working. Therefore, this strength enhancement is required to be considered in the FE modelling explicitly. Previous studies have been conducted to predict the strength enhancement due to the cold-working in stainless steel by Ashraf et al. [27] and Cruise and Gardner [28]. These proposed expressions were used to determine the corner material properties of stainless steel. In the FE modelling, these strength enhancement was introduced to the corner regions as mentioned in Cruise and Gardner [28]. To determine the corner 0.2% proof stress ($\sigma_{0.2,c}$) and corner ultimate stress ($\sigma_{u,c}$) Eqs. (3) [28] and (4) [27] were adopted, respectively. However, the effect of the residual stresses were not taken into account when developing FE models, as it has a negligible effect on the section capacity [5,29].

$$\sigma_{0.2,c} = \frac{1.673\sigma_{0.2,v}}{\left(\frac{r_i}{t}\right)^{0.126}} \quad (3)$$

$$\sigma_{u,c} = 0.75\sigma_{0.2,c} \left(\frac{\sigma_{u,v}}{\sigma_{0.2,v}} \right) \quad (4)$$

where $\sigma_{0.2,v}$ and $\sigma_{u,v}$ are 0.2% proof stress and ultimate stress of virgin material, respectively.

3.5 Loading and boundary conditions

In the experiments simply supported boundary conditions were maintained at the two supports. Thus, a pin and a roller were assigned at the two supports of the beam in the FE models. Also, the rotational degree of freedom about the longitudinal axis (z-axis) of the section was restrained at these two supports to avoid any torsional effect. Suitable boundary conditions were assigned to the flanges at the strap locations to simulate the effect of equal angle straps. The mid-span loading was represented by assigning a vertical displacement to the section at the mid-span and restraining suitable degrees of freedom. Figure 8 illustrates the assigned boundary conditions in the FE models and Table 4 gives the details of boundary conditions used. Note that in Table 4, u_x , u_y and u_z are translations and θ_x , θ_y and θ_z are rotations in the x, y and z directions, respectively while 0 denotes free and 1 denotes restrained conditions.

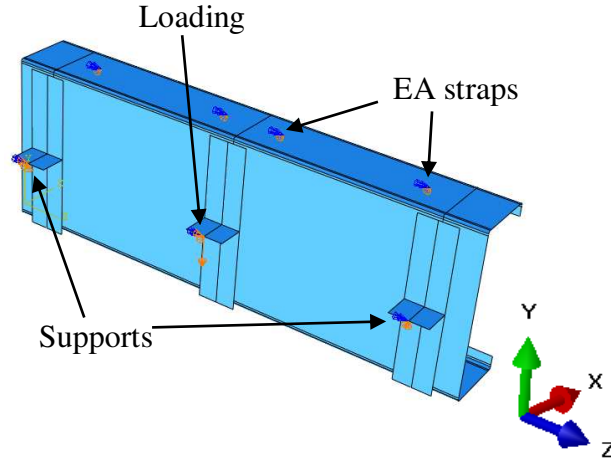


Figure 8: Boundary conditions assigned to the FE models.

259

Table 4: Boundary conditions used in the FE models.

	u_x	u_y	u_z	θ_x	θ_y	θ_z
Left support	1	1	1	0	0	1
Right support	1	1	0	0	0	1
Mid span loading point	1	0	1	0	0	1
Strap locations	1	0	0	0	0	1

260

261 3.6 Geometric imperfections

262 Inclusion of geometric imperfections of thin-walled structures in FE modelling is important as
 263 these geometric imperfections can massively alter the structural behaviour of thin-walled
 264 structures. A study done by Schafer and Pekoz [30] suggested guidelines on treating these
 265 geometric imperfections in numerical modelling. The effect of geometric imperfections to the
 266 non-linear FE models was introduced by following the steps mentioned in [31]. Critical elastic
 267 buckling mode shape was taken as the imperfection pattern of each FE model. In order to define
 268 the imperfection amplitude (ω_0) in the FE modelling modified Dawson and Walker model
 269 [32,33], as given by Eq. (5) was used. This has been previously used by many researchers in
 270 the numerical modelling of stainless steel sections [25,34–36].

$$271 \quad \omega_0 = 0.023 \left(\frac{\sigma_{0.2}}{\sigma_{cr}} \right) t \quad (5)$$

272 where σ_{cr} is the critical elastic buckling stress of the most slender element of the section.

273 3.7 Analysis methods

274 Two analysis types were employed in the current study. For the inclusion of geometric
 275 imperfection patterns in the non-linear FE analysis, a bifurcation buckling analysis was initially
 276 performed and critical elastic buckling mode shapes were identified. Then, the imperfections
 277 were introduced to the non-linear FE models. Thereafter, a non-linear static analysis was
 278 employed on the FE models to study the shear behaviour of LCBs up to failure.

4 Validation

Tables 5 and 6 summarise the comparison of experimental and FE ultimate loads ($V_{Exp.}$ and V_{FE}) of stainless steel and cold-formed steel sections in shear, respectively. The purpose of developing cold-formed steel FE models is discussed later in the Section 5. From the results, it can be seen that developed FE models are able to predict the shear capacity of LCBs with a reasonably good accuracy. The mean and coefficient of variance (COV) of the test to FE shear capacity ratio are 0.99 and 0.070, respectively for the stainless steel sections and 0.99 and 0.084, respectively for the cold-formed steel sections.

Table 5: Comparison of experimental shear capacities with FE results and current design provisions for stainless steel sections.

<i>LCB section</i>	V_{FE} (kN)	$V_{Exp.}/V_{FE}$	$V_{Exp.}/V_{EN1993-1-4}$	$V_{Exp.}/V_{DSM}$
LCB 100×50×15×1.2	16.9	1.09	1.18	1.06
LCB 100×50×15×1.5	24.3	1.01	1.06	1.10
LCB 100×50×15×2.0	35.0	1.03	1.08	1.24
LCB 150×65×15×1.2	20.8	1.04	1.13	1.05
LCB 150×65×15×1.5	29.4	0.89	0.95	0.86
LCB 150×65×15×2.0	42.8	1.02	1.04	0.98
LCB 200×75×15×1.2	23.8	0.97	1.07	1.02
LCB 200×75×15×2.0	52.5	0.90	0.96	0.87
Mean		0.99	1.06	1.02
COV		0.070	0.072	0.122

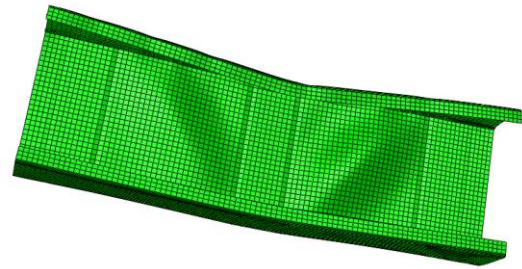
Table 6: Comparison of experimental [12] and FE shear capacities for cold-formed steel sections.

<i>LCB section</i>	$V_{Exp.}$ (kN)	V_{FE} (kN)	V_{Exp}/V_{FE}
LCB 120×50×18×1.5	43.3	47.8	0.91
LCB 120×50×18×2.0	38.1	34.9	1.09
LCB 160×65×15×1.5	54.5	55.2	0.99
LCB 160×65×15×2.0	73.8	77.6	0.95
LCB 200×75×15×1.5	57.0	61.9	0.92
LCB 200×75×15×2.0	55.1	50.1	1.10
Mean			0.99
COV			0.084

In order to demonstrate the ability of the developed FE models to capture the shear failure modes of LCBs, failure modes of stainless steel tests and FE models were compared. Figures 9 and 10 illustrate these comparisons of shear failure modes as captured during the experiment and from the FE model. It can be concluded that the developed FE models were able to capture the failure modes in a fairly similar manner. Further, experimental and FE load-deflection curves for LCB 150×65×15×2.0 are compared in Figure 11. Due to the slip at the bolt connections experimental curve exhibits higher deflections compared to FE curve.

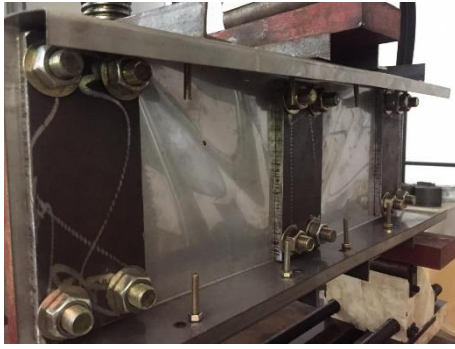


(a) Experiment

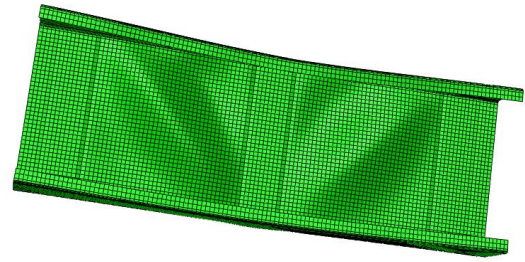


(b) FE model

Figure 9: Shear failure mode of LCB 150×65×15×2.0 section.



(a) Experiment



(b) FE model

Figure 10: Shear failure mode of LCB 200×75×15×1.2 section.

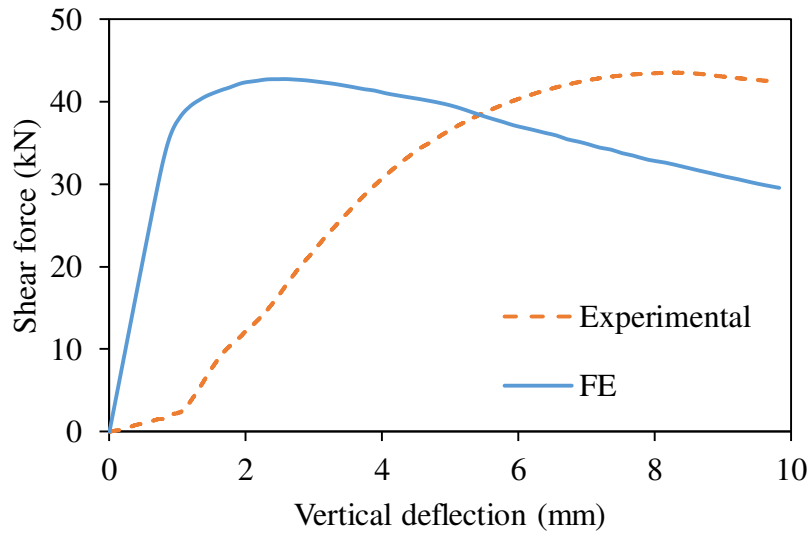


Figure 11: Comparison of experimental and FE load-deflection curves for LCB 150×65×15×2.0 section.

Figure 12 illustrates the FE load-deflection curve for stainless steel LCB 200×75×15×1.2 section obtained without the effect of imperfections. For the FE model without imperfections, a negligible imperfection amplitude ($\omega_0/1000$) was introduced so that there was no considerable effect from the imperfections on the shear behaviour of the section. The lateral deflection of the mid-point of one span (out-of-plane deflection of the web) was monitored against the shear force. Out-of-plane deflection of the web began at Point 1 as it can be seen from the load-deflection curve. Thus, shear force at Point 1 can be taken as the elastic shear buckling load of LCB 200×75×15×1.2 section. Therefore, from Figure 12 elastic shear buckling load of LCB 200×75×15×1.2 section can be taken as 14.92 kN. Using Eq. (18), elastic

shear buckling load of the same section was also calculated and is equal to 15.21 kN, thus demonstrating the ability of developed FE models to capture elastic shear buckling load.

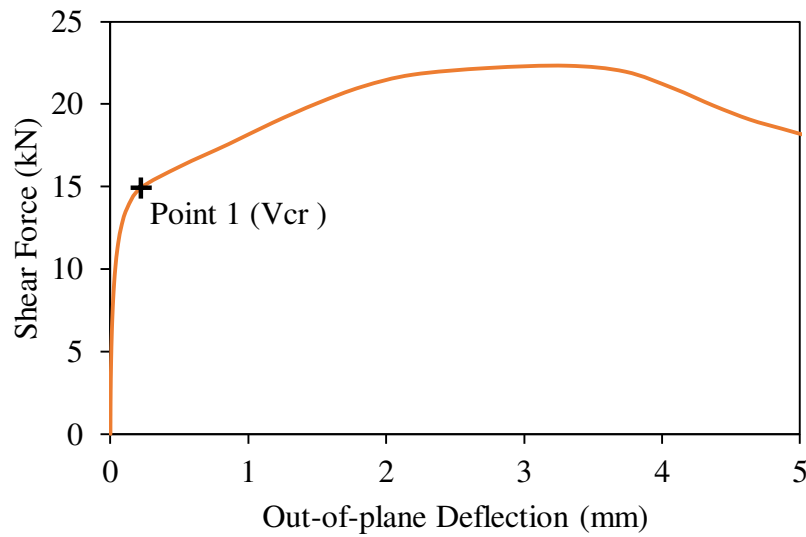
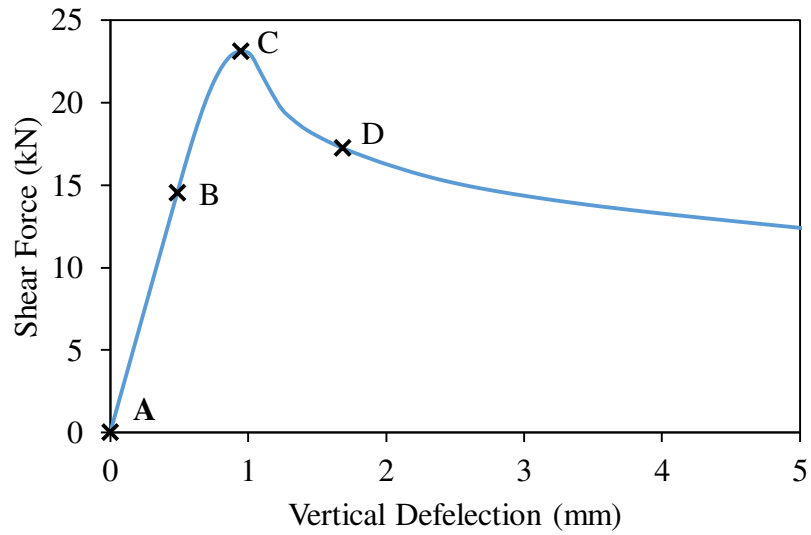
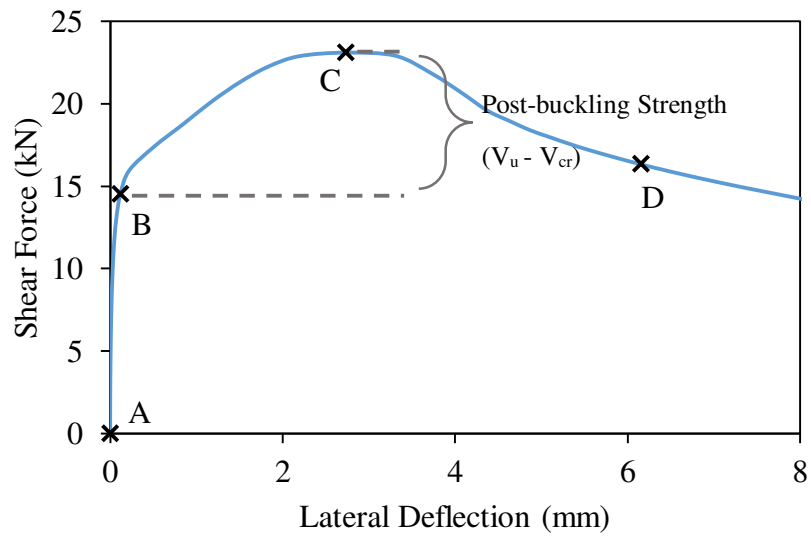


Figure 12: Load-deflection curve for LCB 200×75×15×1.2 section without imperfections.

Figure 13 illustrates the load-vertical deflection curve against the load-lateral deflection curve for the stainless steel LCB 200×75×15×1.2 section without imperfections. It can be seen that there is a considerable amount of post-buckling strength in this section when the web started to buckle out-of-plane at Point B and then reached its shear capacity at point C. The existence of this considerable amount of post-buckling strength particularly in slender LCB sections under shear was also highlighted by Keerthan and Mahendran [12]. Figure 14 shows the FE deformation modes and stress patterns of LCB 200×75×15×1.2 section under progressive loading at points A, B, C and D where these points represent initial, buckling, peak and post-peak conditions, respectively.



(a) Load-vertical deflection curve



(b) Load-lateral deflection curve

Figure 13: Load-deflection curves and post-buckling strength for LCB 200×75×15×1.2 section.

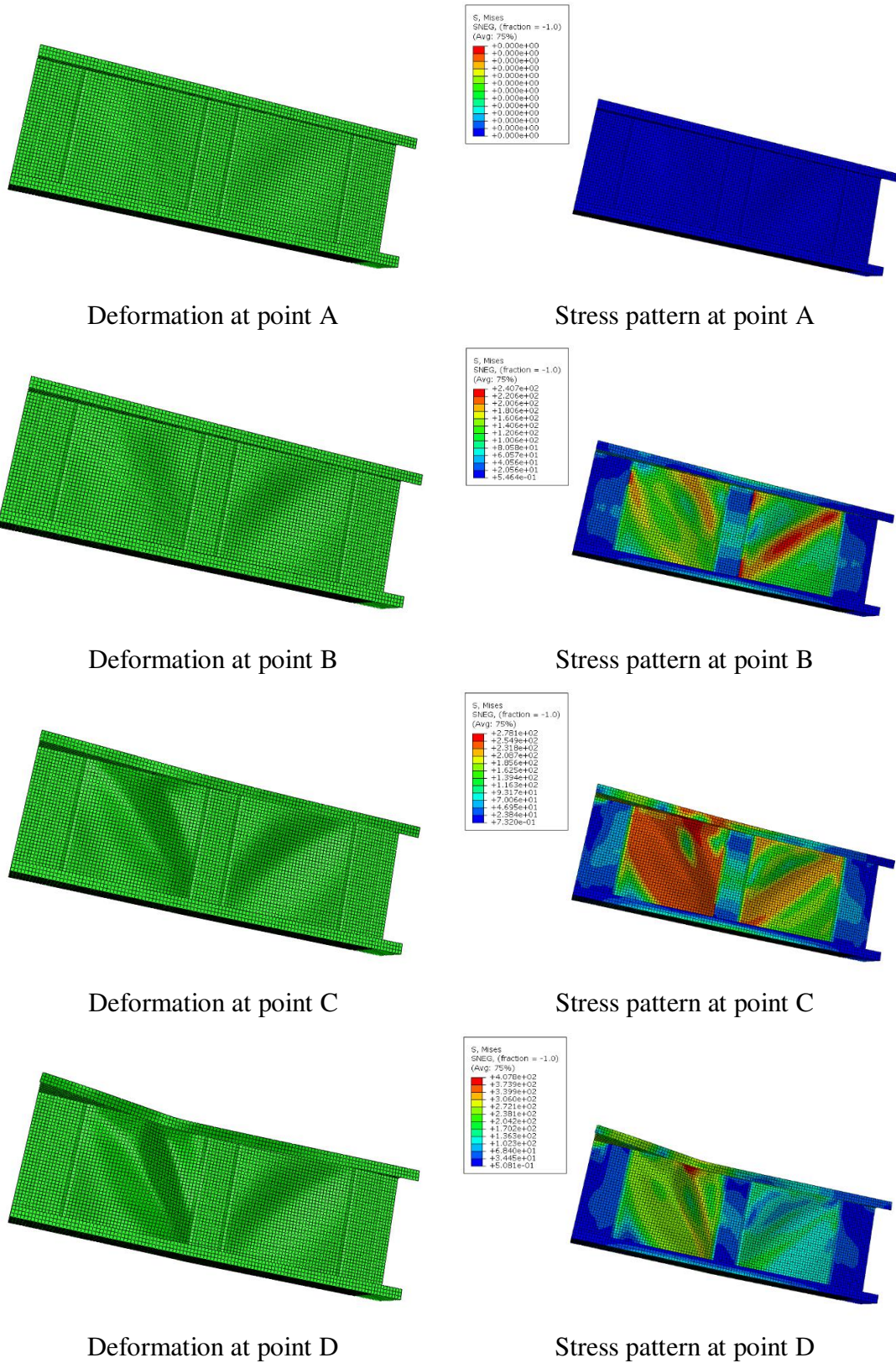


Figure 14: FE deformation modes of LCB 200×75×15×1.2 section under progressive loading.

5 Parametric study

A detailed parametric study was conducted in view of gathering comprehensive database to investigate the shear behaviour of stainless steel LCBs. 100 shear FE models of stainless steel LCBs were developed at this stage. For the parametric study, five different stainless steel grades from EN1993-1-4 [16] including both austenitic and duplex grades were considered. Four different LCB sections and five different thicknesses were selected in order to cover a wide range of slenderness values. The parameters used for the study are summarised in Table 7. The aspect ratio (a/d_1) of 1.0 was used for all FE models developed here. Young's modulus and Poisson's ratio of all stainless steel grades used in the parametric study were taken as 200,000 MPa and 0.3, respectively according to EN1993-1-4 [16]. Tables 8-12 summarise the parametric study results of ultimate shear capacities of cold-formed stainless steel LCBs.

Table 7: Summary of parameters used in the parametric study.

<i>Section</i>	<i>t (mm)</i>	<i>Stainless steel grade</i>	<i>No. of FE models</i>
LCB 100×50×15×t	1, 2, 3, 4, 5	Austenitic- 1.4301,	25
LCB 150×65×15×t		1.4311, 1.4318	25
LCB 200×75×15×t		Duplex- 1.4362,	25
LCB 250×75×15×t		1.4462	25
Total			100

Table 8: Comparison of parametric study results for stainless steel grade 1.4301.

<i>Section</i>	V_{FE} (kN)	$V_{FE}/V_{EN1993-1-4}$	$V_{FE}/V_{EN1993-1-4}$ <i>Proposed</i>	V_{FE}/V_{DSM}	V_{FE}/V_{DSM} <i>Proposed</i>
Stainless steel grade 1.4301					
LCB 100×50×15×1	12.93	1.13	1.11	1.01	1.12
LCB 100×50×15×2	31.37	1.03	1.01	1.18	1.01
LCB 100×50×15×3	56.21	1.25	1.03	1.44	1.03
LCB 100×50×15×4	86.84	1.48	1.06	1.71	1.06
LCB 100×50×15×5	125	1.74	1.13	2.01	1.12
LCB 150×65×15×1	15.28	1.11	1.06	1.04	1.09
LCB 150×65×15×2	39.66	1.02	1.01	0.98	1.01
LCB 150×65×15×3	67.51	0.98	0.97	1.13	0.97
LCB 150×65×15×4	104.21	1.15	1.00	1.33	1.00
LCB 150×65×15×5	143.14	1.28	1.00	1.48	1.00
LCB 200×75×15×1	17.17	1.12	1.05	1.08	1.08
LCB 200×75×15×2	47.90	1.05	1.02	0.94	1.04
LCB 200×75×15×3	81.99	0.94	0.99	1.02	1.00
LCB 200×75×15×4	123.32	1.01	1.00	1.16	1.00
LCB 200×75×15×5	166.53	1.10	0.98	1.27	0.98
LCB 250×75×15×1	18.44	1.12	1.04	1.08	1.05
LCB 250×75×15×2	53.16	1.04	1.01	0.96	1.03
LCB 250×75×15×3	92.38	0.99	0.98	0.91	0.99
LCB 250×75×15×4	138.29	0.90	0.98	1.04	0.98
LCB 250×75×15×5	187.86	0.98	0.97	1.13	0.97
Mean		1.12	1.02	1.20	1.03
COV		0.177	0.042	0.234	0.046

Table 9: Comparison of parametric study results for stainless steel grade 1.4311.

<i>Section</i>	V_{FE} (kN)	$V_{FE}/V_{EN1993-1-4}$	$V_{FE}/V_{EN1993-1-4}$ <i>Proposed</i>	V_{FE}/V_{DSM}	V_{FE}/V_{DSM} <i>Proposed</i>
Stainless steel grade 1.4311					
LCB 100×50×15×1	15.47	1.14	1.10	1.04	1.13
LCB 100×50×15×2	38.14	0.99	1.03	1.14	1.03
LCB 100×50×15×3	65.23	1.15	0.99	1.33	0.99
LCB 100×50×15×4	96.47	1.30	0.99	1.51	0.98
LCB 100×50×15×5	137.98	1.53	1.04	1.76	1.03
LCB 150×65×15×1	17.89	1.10	1.05	1.05	1.08
LCB 150×65×15×2	48.6	1.04	1.03	0.96	1.03
LCB 150×65×15×3	81.51	0.94	0.98	1.08	0.98
LCB 150×65×15×4	123.1	1.08	0.98	1.25	0.98
LCB 150×65×15×5	167.28	1.19	0.98	1.37	0.98
LCB 200×75×15×1	19.98	1.11	1.04	1.08	1.06
LCB 200×75×15×2	57.48	1.06	1.03	0.96	1.05
LCB 200×75×15×3	100.71	1.02	1.02	0.99	1.02
LCB 200×75×15×4	146.33	0.95	0.99	1.10	0.99
LCB 200×75×15×5	197.48	1.03	0.97	1.19	0.97
LCB 250×75×15×1	20.99	1.10	1.01	1.07	1.02
LCB 250×75×15×2	63.04	1.05	1.00	0.98	1.03
LCB 250×75×15×3	113.23	1.02	1.00	0.89	1.01
LCB 250×75×15×4	168.89	0.97	1.00	1.00	1.00
LCB 250×75×15×5	225.49	0.94	0.97	1.08	0.97
Mean		1.09	1.01	1.14	1.02
COV		0.127	0.033	0.186	0.039

Table 10: Comparison of parametric study results for stainless steel grade 1.4318.

<i>Section</i>	V_{FE} (kN)	$V_{FE}/V_{EN1993-1-4}$	$V_{FE}/V_{EN1993-1-4}$ <i>Proposed</i>	V_{FE}/V_{DSM}	V_{FE}/V_{DSM} <i>Proposed</i>
Stainless steel grade 1.4318					
LCB 100×50×15×1	17.62	1.13	1.09	1.04	1.12
LCB 100×50×15×2	44.83	0.96	1.04	1.11	1.05
LCB 100×50×15×3	76.98	1.13	1.01	1.30	1.01
LCB 100×50×15×4	113.57	1.27	1.00	1.47	1.00
LCB 100×50×15×5	161.41	1.48	1.05	1.71	1.04
LCB 150×65×15×1	20.26	1.10	1.04	1.05	1.07
LCB 150×65×15×2	56.74	1.05	1.03	0.93	1.04
LCB 150×65×15×3	96	0.92	0.99	1.06	0.99
LCB 150×65×15×4	145.37	1.06	1.00	1.22	1.00
LCB 150×65×15×5	196.74	1.16	0.99	1.34	0.99
LCB 200×75×15×1	22.33	1.10	1.02	1.07	1.04
LCB 200×75×15×2	66.36	1.06	1.03	0.98	1.05
LCB 200×75×15×3	117.87	1.04	1.02	0.96	1.03
LCB 200×75×15×4	173.29	0.93	1.01	1.07	1.01
LCB 200×75×15×5	234.13	1.02	0.99	1.17	1.00
LCB 250×75×15×1	23.48	1.09	1.00	1.06	1.00
LCB 250×75×15×2	72.99	1.06	1.01	1.00	1.04
LCB 250×75×15×3	132.79	1.04	1.01	0.93	1.03
LCB 250×75×15×4	196.61	1.01	1.00	0.97	1.00
LCB 250×75×15×5	267.77	0.92	1.00	1.06	1.00
Mean		1.08	1.02	1.13	1.03
COV		0.119	0.024	0.175	0.030

Table 11: Comparison of parametric study results for stainless steel grade 1.4362.

<i>Section</i>	V_{FE} (kN)	$V_{FE}/V_{EN1993-1-4}$	$V_{FE}/V_{EN1993-1-4}$ <i>Proposed</i>	V_{FE}/V_{DSM}	V_{FE}/V_{DSM} <i>Proposed</i>
Stainless steel grade 1.4362					
LCB 100×50×15×1	20.63	1.10	1.06	1.03	1.09
LCB 100×50×15×2	53.96	0.99	1.03	1.04	1.03
LCB 100×50×15×3	89.5	1.02	0.97	1.18	0.97
LCB 100×50×15×4	129.49	1.13	0.94	1.30	0.94
LCB 100×50×15×5	174.25	1.24	0.93	1.43	0.93
LCB 150×65×15×1	23.8	1.09	1.02	1.05	1.05
LCB 150×65×15×2	70.09	1.08	1.05	0.97	1.06
LCB 150×65×15×3	116.54	0.95	0.99	1.00	0.99
LCB 150×65×15×4	171.32	0.97	0.97	1.12	0.97
LCB 150×65×15×5	226.62	1.04	0.94	1.20	0.94
LCB 200×75×15×1	25.71	1.08	1.00	1.05	1.01
LCB 200×75×15×2	79.53	1.06	1.02	0.99	1.05
LCB 200×75×15×3	146.65	1.06	1.04	0.93	1.05
LCB 200×75×15×4	212.11	0.97	1.01	1.02	1.02
LCB 200×75×15×5	277.55	0.94	0.97	1.08	0.97
LCB 250×75×15×1	26.4	1.05	0.96	1.02	0.95
LCB 250×75×15×2	87.15	1.06	1.01	1.02	1.04
LCB 250×75×15×3	159.6	1.03	1.00	0.94	1.02
LCB 250×75×15×4	245.71	1.04	1.02	0.94	1.03
LCB 250×75×15×5	321.48	0.94	0.98	0.99	0.99
Mean		1.04	0.99	1.07	1.00
COV		0.070	0.038	0.119	0.047

Table 12: Comparison of parametric study results for stainless steel grade 1.4462.

<i>Section</i>	V_{FE} (kN)	$V_{FE}/V_{EN1993-1-4}$	$V_{FE}/V_{EN1993-1-4}$ <i>Proposed</i>	V_{FE}/V_{DSM}	V_{FE}/V_{DSM} <i>Proposed</i>
Stainless steel grade 1.4462					
LCB 100×50×15×1	22.32	1.11	1.06	1.04	1.09
LCB 100×50×15×2	58.97	1.03	1.04	1.02	1.04
LCB 100×50×15×3	98.09	1.00	0.98	1.16	0.98
LCB 100×50×15×4	140.72	1.10	0.94	1.27	0.94
LCB 100×50×15×5	188.3	1.21	0.92	1.39	0.92
LCB 150×65×15×1	25.52	1.09	1.02	1.05	1.04
LCB 150×65×15×2	75.59	1.07	1.04	0.97	1.06
LCB 150×65×15×3	127.68	0.99	1.00	0.99	1.00
LCB 150×65×15×4	186.87	0.95	0.97	1.10	0.98
LCB 150×65×15×5	245.93	1.01	0.94	1.17	0.94
LCB 200×75×15×1	27.1	1.06	0.98	1.04	0.99
LCB 200×75×15×2	86.63	1.08	1.03	1.01	1.06
LCB 200×75×15×3	160.23	1.07	1.05	0.96	1.06
LCB 200×75×15×4	230.56	1.00	1.01	1.00	1.02
LCB 200×75×15×5	302.5	0.92	0.97	1.06	0.97
LCB 250×75×15×1	27.55	1.02	0.94	0.99	0.92
LCB 250×75×15×2	93.61	1.06	1.00	1.02	1.03
LCB 250×75×15×3	174.2	1.04	1.01	0.96	1.03
LCB 250×75×15×4	267.71	1.04	1.02	0.92	1.04
LCB 250×75×15×5	356.07	0.99	1.00	0.99	1.00
Mean		1.04	1.00	1.06	1.01
COV		0.060	0.040	0.109	0.049

395 Due to the pronounced strain hardening effect of stainless steel, significant strength increment
396 can be envisaged beyond the yield strength of the material which is conventionally taken as the
397 0.2 % proof stress. In order to highlight this strain hardening effect on the shear behaviour of
398 stainless steel LCBs, further analysis was conducted. Both compact sections and slender

sections were considered here. The shear capacities of twenty LCBs of stainless steel grade 1.4301 was compared with the results obtained from cold-formed LCBs. The validated cold-formed steel FE models were incorporated for this purpose. When developing cold-formed steel FE models stress was limited to the yield stress of grade 1.4301. Table 13 summarises the shear capacities and percentage increment of strength for each section where $\bar{\lambda}_w$ is the web slenderness calculated from EN1993-1-4 [16].

Table 13: Comparison of shear capacities of stainless steel and cold-formed steel LCBs.

<i>Section</i>	<i>t</i> (mm)	<i>d_l/t</i>	$\bar{\lambda}_w$	<i>V_{stainless steel}</i> (kN)	<i>V_{cold-formed steel}</i> (kN)	% <i>Increment</i>
LCB 100×50×15×1	1.0	98.0	0.87	12.93	12.28	5.29
LCB 100×50×15×2	2.0	48.0	0.43	31.37	25.51	22.97
LCB 100×50×15×3	3.0	31.3	0.28	56.21	40.39	39.17
LCB 100×50×15×4	4.0	23.0	0.20	86.84	58.38	48.75
LCB 100×50×15×5	5.0	18.0	0.16	125	77.89	60.48
LCB 150×65×15×1	1.0	148.0	1.31	15.28	15.01	1.80
LCB 150×65×15×2	2.0	73.0	0.65	39.66	36.13	9.77
LCB 150×65×15×3	3.0	48.0	0.43	67.51	56.13	20.27
LCB 150×65×15×4	4.0	35.5	0.31	104.21	77.94	33.71
LCB 150×65×15×5	5.0	28.0	0.25	143.14	101.04	41.67
LCB 200×75×15×1	1.0	198.0	1.76	17.17	16.92	1.48
LCB 200×75×15×2	2.0	98.0	0.87	47.9	45.43	5.44
LCB 200×75×15×3	3.0	64.7	0.57	81.99	72.74	12.72
LCB 200×75×15×4	4.0	48.0	0.43	123.32	100.01	23.31
LCB 200×75×15×5	5.0	38.0	0.34	166.53	127.82	30.28
LCB 250×75×15×1	1.0	248.0	2.20	18.44	18.08	1.99
LCB 250×75×15×2	2.0	123.0	1.09	53.16	52.27	1.70
LCB 250×75×15×3	3.0	81.3	0.72	92.38	84.44	9.40
LCB 250×75×15×4	4.0	60.5	0.54	138.29	118.78	16.43
LCB 250×75×15×5	5.0	48.0	0.43	187.86	152.99	22.79

According to Table 13, it can be seen that when d_1/t_w ratio is less than 28, more than 40 % shear capacity increment can be expected in stainless steel sections due to the effect of strain hardening. Therefore, it is concluded that this strain hardening effect is more pronounced in compact sections while that for slender sections is negligible. This strength increment existing in compact sections is known as inelastic reserve capacity. Similar inelastic reserve capacities were observed for the stainless steel rectangular hollow sections in shear by Sonu and Singh [25]. This effect is further highlighted for stainless steel angles and channels in bending by Theofanous et al. [4]. This shear capacity increment in compact sections due to the strain hardening of stainless steel is further highlighted from Figure 15 where sectional shear capacity (V_u) to yield load (V_y) ratio was compared with the web slenderness ($\bar{\lambda}_w$).

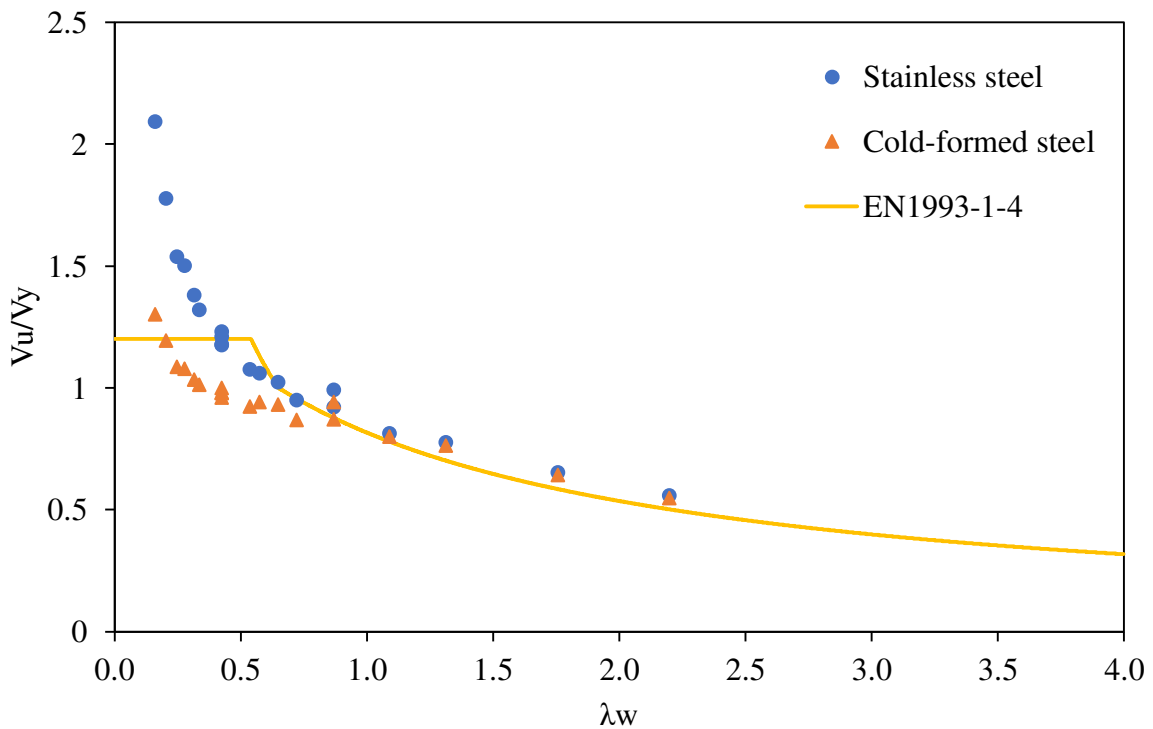


Figure 15: Comparison of shear capacities of stainless steel and cold-formed steel LCBs.

6 Current shear design rules

6.1 EN1993-1-4 [16] shear design rules

EN1993-1-4 [16] is based on the effective width method where traditional cross-section classification approach is used to divide cross sections into different behavioural classes by assuming the class of its most slender element while incorporating the effect of material properties, support conditions and loading patterns. Design provisions for shear introduced in EN1993-1-4 [16] are to be referred alongside with the provisions provided in EN1993-1-1 [37] and EN1993-1-5 [17]. Eq. (6) has been introduced in EN1993-1-4 [16] to calculate the sectional shear resistance ($V_{b,Rd}$) which is taken as the sum of web shear resistance ($V_{bw,Rd}$) and flange shear resistance ($V_{bf,Rd}$).

$$V_{b,Rd} = V_{bw,Rd} + V_{bf,Rd} \leq \frac{\eta f_{yw} h_w t_w}{\sqrt{3} \gamma_{M1}} \quad (6)$$

where, f_{yw} is the web yield stress, h_w is the clear web depth between flanges and t_w is the web thickness. Here $\eta = 1.2$ is recommended and γ_{M1} is a partial factor [16].

Eq. (7) gives the web shear resistance, $V_{bw,Rd}$ where χ_w is the web shear buckling reduction factor, values for which for webs with rigid end-post are given in Table 14.

$$V_{bw,Rd} = \frac{\chi_w f_{yw} h_w t_w}{\sqrt{3} \gamma_{M1}} \quad (7)$$

Table 14: Web shear buckling reduction factor, χ_w for webs with rigid end post according to EN1993-1-4 [16].

χ_w	
$\bar{\lambda}_w \leq 0.65/\eta$	η
$0.65/\eta < \bar{\lambda}_w < 0.65$	$0.65/\bar{\lambda}_w$
$\bar{\lambda}_w \geq 0.65$	$1.56/(0.91 + \bar{\lambda}_w)$

In Table 14, $\bar{\lambda}_w$ is the web slenderness which is defined in Eq. (8) for webs with transverse stiffeners at supports and mid span where ε and k_τ are material factor and web shear buckling coefficient, respectively.

$$\bar{\lambda}_w = \frac{h_w}{37.4 t_w \varepsilon \sqrt{k_\tau}} \quad (8)$$

Material factor (ε) is defined by Eq. (9) while web shear buckling coefficient (k_τ) for plates with rigid transverse stiffeners and without longitudinal stiffeners is given by Eqs. (10) and (11) where f_y is the yield stress, E is the modulus of elasticity and a is the distance between transverse stiffeners.

$$\varepsilon = \sqrt{\frac{235}{f_y} \frac{E}{210\,000}} \quad (9)$$

$$k_\tau = 5.34 + \frac{4.00}{(a/h_w)^2} \text{ for } \frac{a}{h_w} \geq 1 \quad (10)$$

$$k_\tau = 4.00 + \frac{5.34}{(a/h_w)^2} \text{ for } \frac{a}{h_w} < 1 \quad (11)$$

Flange shear resistance ($V_{bf,Rd}$) given in Eq. (6) is defined by Eq. (12) where b_f and t_f are flange width and thickness, respectively which provides the least axial resistance while f_{yf} is the flange yield stress. Here c is given in Eq. (13). It is of note that Eq. (12) is only valid if $M_{Ed} < M_{f,Rd}$ where M_{Ed} is the design bending moment and $M_{f,Rd}$ is the effective flange moment resistance.

$$V_{bf,Rd} = \frac{b_f t_f^2 f_{yf}}{c \gamma_{M1}} \left(1 - \left(\frac{M_{Ed}}{M_{f,Rd}} \right)^2 \right) \quad (12)$$

$$c = a \left[0.17 + \frac{3.5 b_f t_f^2 f_{yf}}{t_w h_w^2 f_{yw}} \right] \text{ and } \frac{c}{a} \leq 0.65 \quad (13)$$

6.2 Direct strength method (DSM)

The direct strength method is an alternative to the conventional effective width method [38]. The accurate member elastic stability is the fundamental theory on which DSM is formed where the strength of a section is calculated considering all the elastic instabilities of the gross cross section [39]. In DSM design resistance equations, the strength of a cross-section is defined as a function of overall slenderness of the cross section (λ). DSM shear capacity (V_v) prediction equations proposed by Pham and Hancock [40] are given in Eqs. (14) and (15) where two equations represent the shear yielding, and elastic and inelastic shear buckling regions, respectively while λ is defined as in Eq. (16).

$$\frac{V_v}{V_y} = 1 \text{ for } \lambda \leq 0.815 \quad (14)$$

$$\frac{V_y}{V_{cr}} = \left[1 - 0.15 \left(\frac{1}{\lambda^2} \right)^{0.4} \right] \left(\frac{1}{\lambda^2} \right)^{0.4} \text{ for } \lambda > 0.815 \quad (15)$$

where

$$\lambda = \sqrt{\frac{V_y}{V_{cr}}} \quad (16)$$

When calculating λ , shear yield capacity (V_y) and elastic shear buckling capacity (V_{cr}) are taken as defined by Eqs. (17) and (18), respectively.

$$V_y = 0.6 f_{yw} d_1 t_w \quad (17)$$

$$V_{cr} = \frac{k \pi^2 E t_w^3}{12 (1 - \nu^2) d_1} \quad (18)$$

where f_{yw} is the web yield stress, d_1 is the flat depth of the web, t_w is the web thickness, E is the Young's modulus and ν is the Poisson's ratio. Here k is the shear buckling coefficient of the section. Keerthan and Mahendran [12] proposed a set of equations (Eqs. (19)-(23)) to calculate the shear buckling coefficient, k of LCBs considering the additional fixity available at the web-flange juncture of LCBs.

$$k = k_{ss} + 0.23(k_{sf} - k_{ss}) \quad (19)$$

$$k_{ss} = 5.34 + \frac{4}{(a/d_1)^2} \text{ for } \frac{a}{d_1} \geq 1 \quad (20)$$

$$k_{ss} = 4 + \frac{5.34}{(a/d_1)^2} \text{ for } \frac{a}{d_1} < 1 \quad (21)$$

$$k_{sf} = 8.98 + \frac{5.61}{(a/d_1)^2} - \frac{1.99}{(a/d_1)^3} \text{ for } \frac{a}{d_1} \geq 1 \quad (22)$$

$$k_{sf} = \frac{5.34}{(a/d_1)^2} + \frac{2.31}{(a/d_1)} - 3.44 + \frac{8.39}{(a/d_1)} \text{ for } \frac{a}{d_1} < 1 \quad (23)$$

6.3 Performance of current design rules

The experimental results and developed shear FE models of stainless steel LCBs were utilised to assess the applicability of EN1993-1-4 [16] and DSM shear design rules described in the above sections. Table 5 includes the comparison of current shear design rules discussed here with the experimental results while Tables 8-12 compare the performance of the current EN1993-1-4 [16] and DSM shear design rules with the obtained FE results from the parametric study. The results show that experimental and FE shear capacities to predicted shear capacities

ratio has a mean and COV of 1.07 and 0.118, respectively for the current EN1993-1-4 [16] predictions while that for the current DSM predictions are 1.11 and 0.176, respectively. Moreover, Figures 16 and 17 illustrate the comparison of experimental and FE shear capacities with the current EN1993-1-4 [16] and DSM shear design curves, respectively. From both comparisons it is evident that the existing shear design rules are too conservative in particularly for compact sections.

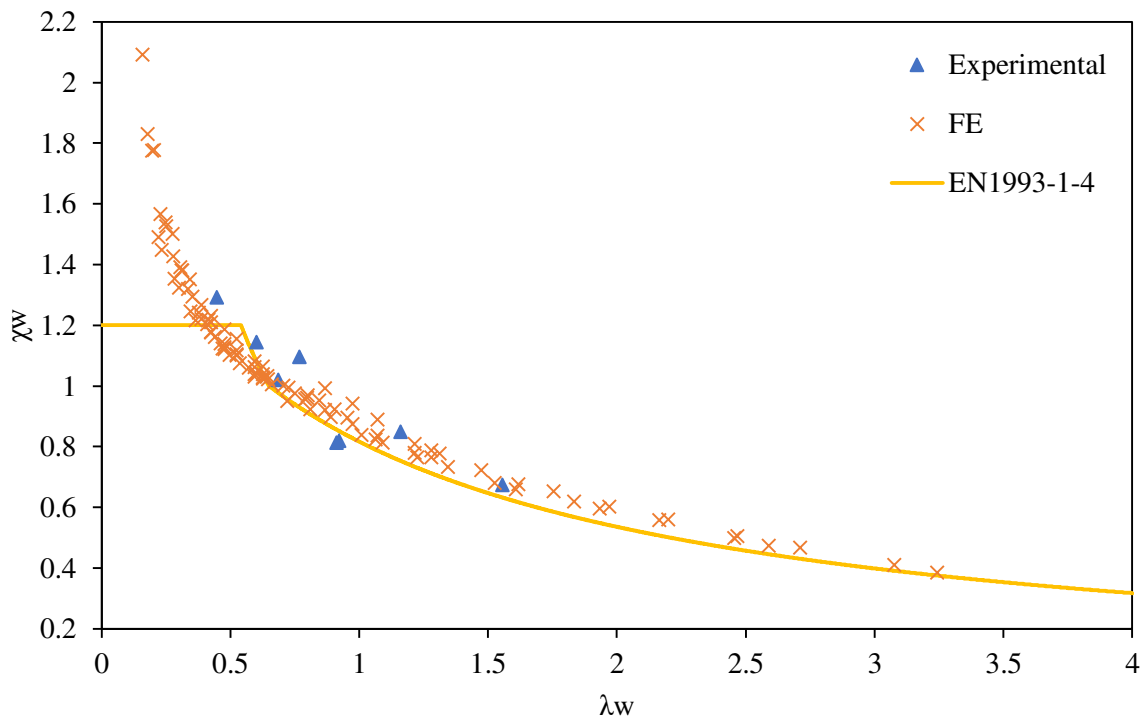


Figure 16: Comparison of experimental and FE shear capacities with the current EN1993-1-4 [16] shear capacity prediction curve.

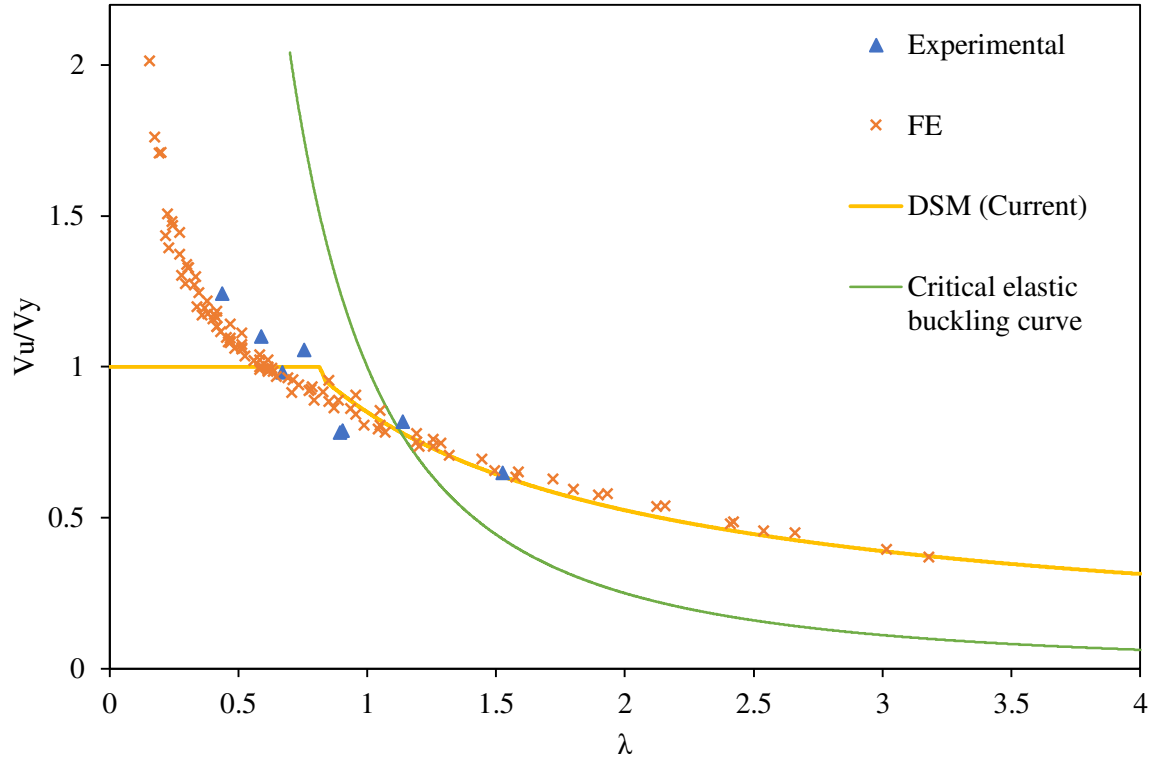


Figure 17: Comparison of experimental and FE shear capacities with the current DSM shear capacity prediction curve.

7 Proposed shear design rules

In order to address the previously discussed shortcomings present in the current EN1993-1-4 [16] and DSM shear design provisions, attempts were made to modify the shear design rules while aiming to improve the prediction accuracy. When developing such design rules, special attention was given to capture the pronounced inelastic reserve capacity in compact stainless steel LCBs in shear.

7.1 Proposed EN1993-1-4 [16] shear design rules

The applicability of the current shear design rules to predict shear behaviour of stainless steel LCBs was evaluated and required modifications were made to Eqs. (6)-(13) given in Section 6.1 in view of enhancing the prediction accuracy. For the calculation of sectional shear resistance ($V_{b,Rd}$) using Eq. (6), the flange shear resistance ($V_{bf,Rd}$) is required to be taken into account as given by Eq. (12). Therefore, required modifications were made to the web shear buckling coefficient (χ_w) in Eq. (7) by comparing the web shear resistance ($V_{bw,Rd}$) with the

flange shear resistance reduced FE and experimental shear capacities ($V_{FE} (& Exp.) - V_{bf,Rd}$). However, it is worth to note that for almost all the sections studied, the condition $M_{Ed} < M_{f,Rd}$ was not satisfied while for very few sections this condition was satisfied, but yet for those sections flange shear resistance ($V_{bf,Rd}$) was negligible.

A set of expressions were proposed for the web shear buckling coefficient (χ_w) as functions of web slenderness ($\bar{\lambda}_w$) following a regression analysis. For the sections failed below their yield load, a separate expression was proposed while for the sections achieve a greater strength above their yield load due to the pronounced strain hardening effect of stainless steel, another separate expression was proposed with an upper limit based on the FE results. Table 15 summarises the expressions proposed herein for the web shear buckling coefficient (χ_w) while all experimental and FE data points are compared with the proposed EN1993-1-4 [16] curve for the web shear buckling coefficient (χ_w) in Figure 18.

Table 15: Proposed web shear buckling reduction factor, χ_w for webs with rigid end post for EN1993-1-4 [16].

	χ_w
$\bar{\lambda}_w \leq 0.12$	2.1
$0.12 < \bar{\lambda}_w < 0.667$	$0.839/\bar{\lambda}_w^{0.433}$
$\bar{\lambda}_w \geq 0.667$	$1.797/(1.13 + \bar{\lambda}_w)$

From Figure 18, it can be seen that proposed expressions for the web shear buckling coefficient (χ_w) in EN1993-1-4 [16] considering stainless steel LCBs, were able to capture the shear capacity well throughout the web slenderness ($\bar{\lambda}_w$) range. From Table 16, it is highlighted that compared to the current EN1993-1-4 [16] shear design provisions, proposed expressions enhance the prediction accuracy specially in the compact region ($\bar{\lambda}_w < 0.667$) emphasising the ability to capture the inelastic reserve capacity available in stainless steel LCBs in shear.

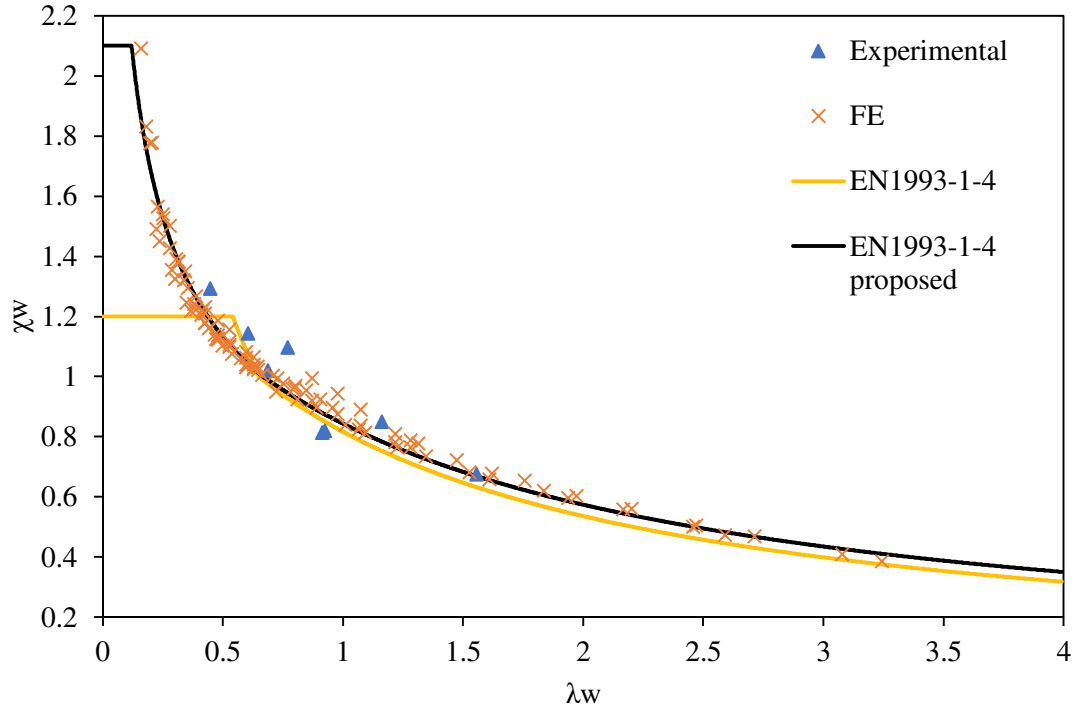


Figure 18: Comparison of experimental and FE shear capacities with proposed curve for web shear buckling coefficient (χ_w).

Table 16: Comparison of FE and experimental shear capacities with EN1993-1-4 [16] predictions.

	$V_{FE \text{ (\& Exp.)}} / V_{EN1993-1-4}$	$V_{FE \text{ (\& Exp.)}} / V_{EN1993-1-4}$ <i>Proposed</i>
$\bar{\lambda}_w < 0.667$		
Mean	1.07	1.00
COV	0.157	0.039
$\bar{\lambda}_w \geq 0.667$		
Mean	1.07	1.02
COV	0.040	0.041
Overall		
Mean	1.07	1.01
COV	0.118	0.042

7.2 Proposed DSM shear design rules

In this section modifications made to the current DSM shear design provisions to enhance the shear capacity prediction accuracy of stainless steel LCBs are detailed. Firstly, using Eqs. (14)-(23), applicability of the current provisions were assessed and then Eq. (15) was recalibrated and fitted to the experimental and FE data points by following a regression analysis. Furthermore, another equation was proposed to capture the inelastic reserve capacity of the compact sections with an upper limit. Therefore, this study suggests Eqs. (24)-(26) to be employed instead of Eqs. (14) and (15) in the DSM shear design provisions for stainless steel LCBs.

$$\frac{V_v}{V_y} = 2 \text{ for } \lambda \leq 0.122 \quad (24)$$

$$\frac{V_v}{V_y} = \frac{0.795}{\lambda^{0.439}} \text{ for } 0.122 < \lambda \leq 0.592 \quad (25)$$

$$\frac{V_v}{V_y} = \left[1 - 0.213 \left(\frac{1}{\lambda^2} \right)^{0.35} \right] \left(\frac{1}{\lambda^2} \right)^{0.35} \text{ for } \lambda > 0.592 \quad (26)$$

where all the notations are defined in the Section 6.2.

Table 17: Comparison of FE and experimental shear capacities with DSM predictions.

	$V_{FE \text{ (} \& \text{ Exp.)}} / V_{DSM}$	$V_{FE \text{ (} \& \text{ Exp.)}} / V_{DSM}$ <i>Proposed</i>
$\bar{\lambda}_w \leq 0.592$		
Mean	1.24	1.00
COV	0.175	0.040
$\bar{\lambda}_w > 0.592$		
Mean	1.00	1.04
COV	0.054	0.043
Overall		
Mean	1.11	1.02
COV	0.176	0.047

Current and proposed DSM shear capacity predictions are also compared in Table 17. From Table 17, it can be seen that the newly proposed shear design equations significantly enhance the prediction accuracy over the existing shear design equations. Also, unlike the existing provisions, the new provisions are able to predict the inelastic reserve capacity of compact sections. Figure 19 illustrates the comparison of experimental and FE shear capacities for stainless steel LCBs against the newly proposed DSM design curve. In addition, the critical elastic shear buckling curve is included in Figure 19 to demonstrate the available post-buckling strength in slender sections.

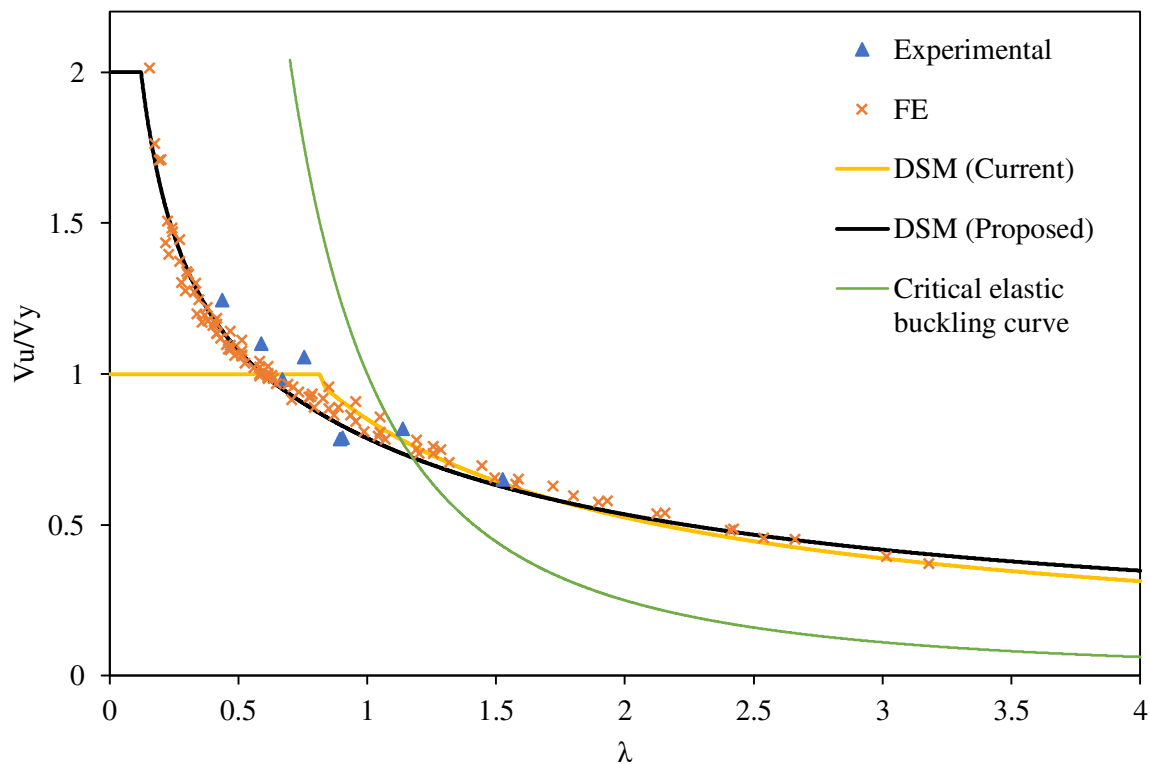


Figure 19: Comparison of experimental and FE shear capacities with proposed DSM shear design curve.

7.3 Reliability analysis

In order to assess the applicability of proposed EN1993-1-4 [16] and DSM shear design rules a reliability analysis was carried out by following the method suggested in North American specification for cold-formed steel structures [41]. In this method the capacity reduction factor

(ϕ_v) is calculated considering the effect of material and geometric variations as given by Eq. (27).

$$\phi_v = 1.52 M_m F_m P_m e^{-\beta_0 \sqrt{(V_m^2 + V_f^2 + C_p V_p^2 + V_q^2)}} \quad (27)$$

where M_m and V_m are the mean and COV of the material factor, respectively and taken as 1.1 and 0.1, respectively. F_m and V_f are the mean and COV of the fabrication factor, respectively and taken as 1.0 and 0.05, respectively. P_m and V_p (not less than 0.065) are the mean and COV of the experimental or FE to predicted ratio, respectively. V_q is the COV of the load effect taken as 0.21. β_0 is the target reliability index taken as 2.5. C_p is the correction factor and is calculated using Eq. (28).

$$C_p = \left[1 + \frac{1}{n} \right] \left[\frac{m}{m-2} \right] \quad (28)$$

where n is the number of data points and m is the number of degrees of freedom, taken as $n-1$.

Considering all the experiments and FE models for stainless steel LCBs in shear reliability of the proposed design rules were assessed. For the proposed EN1993-1-4 [16] design rules taking $P_m=1.01$ (from Table 16) and $V_p=0.065$ (recommended minimum value) resulted in $\phi_v=0.91$. And for the developed DSM shear design rules adopting $P_m=1.02$ (from Table 17) and $V_p=0.065$ (recommended minimum value) resulted in $\phi_v=0.92$. Therefore, for both proposals a capacity reduction factor (ϕ_v) of 0.90 is recommended.

8 Concluding remarks

This paper presents the details of testing and numerical modelling of stainless steel LCBs in shear. Developed FE models were validated using the test results and highlighted the capability of FE models to predict shear capacities, elastic shear buckling loads, and failure modes with a reasonably good accuracy. From the FE results, it is also highlighted that there is significant post-buckling strength in slender stainless steel LCBs in shear. The FE models of cold-formed steel LCBs in shear were also developed and validated. Employing these cold-formed steel and stainless steel FE models, inelastic reserve capacity envisaged in compact stainless steel LCBs in shear was highlighted. It has been shown that when d_1/t ratio is less than 28, more than 40 % strength increment exists in compact sections due to the strain hardening effect of stainless steel. 100 stainless steel FE models were developed using the validated FE models in order to assess the applicability of current EN1993-1-4 [16] and DSM shear design rules for the

stainless steel LCBs. Current shear design rules were found to be too conservative specially for compact sections. Therefore, existing shear design rules were then modified to enhance the prediction accuracy. A set of expressions to predict web shear buckling coefficient (χ_w) in EN1993-1-4 [16] were proposed while detailing the modified and new equations for DSM shear design rules. It is worth to note that both proposed EN1993-1-4 [16] and DSM shear design rules are able to capture the available inelastic reserve capacity in compact stainless steel LCBs, unlike the existing shear design rules. However, more experimental data on the inelastic reserve capacity is recommended and is currently underway by the authors to enhance the understanding of this behaviour in compact sections.

References

- [1] N. Baddoo, Designing Structural Stainless Steel Members To Eurocode 3, New steel construction, April, 2009.
- [2] SCI, Design Manual for Structural Stainless Steel, Fourth edition, SCI Publication No. P413, The Steel Construction Institute, Ascot, UK, 2017.
- [3] L. Gardner, M. Theofanous, Discrete and continuous treatment of local buckling in stainless steel elements, Journal of Constructional Steel Research. 64 (11) (2008) 1207–1216.
- [4] M. Theofanous, A. Liew, L. Gardner, Experimental study of stainless steel angles and channels in bending, Structures. 4 (2015) 80–90.
- [5] Y. Liang, O. Zhao, Y. Long, L. Gardner, Stainless steel channel sections under combined compression and minor axis bending – Part 1: Experimental study and numerical modelling, Journal of Constructional Steel Research. 152 (2019) 154–161.
- [6] Y. Liang, O. Zhao, Y. Long, and L. Gardner, Stainless steel channel sections under combined compression and minor axis bending – Part 2: Parametric studies and design, Journal of Constructional Steel Research. 152 (2019) 162–172.
- [7] O. Zhao, L. Gardner, The continuous strength method for the design of mono-symmetric and asymmetric stainless steel cross-sections in bending, Journal of Constructional Steel Research. 150 (2018) 141–152.
- [8] S. Niu, K. J. R. Rasmussen, F. Fan, Distortional-global interaction buckling of stainless steel C-beams: Part II - Numerical study and design, Journal of Constructional Steel Research. 96 (2014) 40–53.

- [9] S. Niu, K. J. R. Rasmussen, F. Fan, Distortional-global interaction buckling of stainless steel C-beams: Part I - Experimental investigation, *Journal of Constructional Steel Research*. 96 (2014) 127–139.
- [10] S. Fan, M. Chen, S. Li, Z. Ding, G. Shu, B. Zheng, Stainless steel lipped C-section beams: Numerical modelling and development of design rules, *Journal of Constructional Steel Research*. 152 (2019) 29–41.
- [11] P. Keerthan, M. Mahendran, Experimental studies on the shear behaviour and strength of LiteSteel beams, *Engineering Structures*. 32 (10) (2010) 3235–3247.
- [12] P. Keerthan, M. Mahendran, Experimental investigation and design of lipped channel beams in shear, *Thin-Walled Structures*. 86 (2015) 174–184.
- [13] P. Keerthan, M. Mahendran, Improved shear design rules of cold-formed steel beams, *Engineering Structures*. 99 (2015) 603–615.
- [14] C. H. Pham, G. J. Hancock, Experimental investigation of high strength cold-formed C-section in combined bending and shear, *Journal of Structural Engineering*. 136 (7) (2010) 866–878.
- [15] C. H. Pham, G. J. Hancock, Numerical simulation of high strength cold-formed purlins in combined bending and shear, *Journal of Constructional Steel Research*. 66 (10) (2010) 1205–1217.
- [16] EN 1993-1-4:2006+A1:2015. Eurocode 3 – Design of steel structures – Part 1 – 4: General rules – Supplementary rules for stainless steels, European Committee for Standardization (CEN), Brussels, 2015.
- [17] EN 1993-1-5. Eurocode 3 – Design of steel structures – Part 1 – 5: Plated structural elements, European Committee for Standardization (CEN), Brussels, 2006.
- [18] AS/NZS 4673. Cold-formed stainless steel structures, AS/NZS 4673:2001, Sydney, 2001.
- [19] SEI/ASCE 8–02. Specification for the design of cold-formed stainless steel structural members, American Society of Civil Engineers (ASCE), Reston, 2002.
- [20] S. Afshan, L. Gardner, The continuous strength method for structural stainless steel design, *Thin-Walled Structures*. 68 (2013) 42–49.
- [21] O. Zhao, S. Afshan, L. Gardner, Structural response and continuous strength method design of slender stainless steel cross-sections, *Engineering Structures*. 140 (2017) 14–25.
- [22] V. V. Nguyen, G. J. Hancock, C. H. Pham, Development of the Thin-Wall-2 program for buckling analysis of thin-walled sections under generalised loading, *Proceedings of*

- the eighth international conference on advances in steel structures, Lisbon, Portugal, 2015.
- [23] P. Keerthan, M. Mahendran, D. Hughes, Numerical studies and design of hollow flange channel beams subject to combined bending and shear actions, *Engineering Structures*. 75 (2014) 197–212.
- [24] ABAQUS 6.14 Analysis User's Guide Volume IV: Elements, Dassault Systèmes, Rhode Island, USA, 2014.
- [25] J. K. Sonu, K. D. Singh, Shear characteristics of Lean Duplex Stainless Steel (LDSS) rectangular hollow beams, *Structures*. 10 (2016) 13–29.
- [26] I. Arrayago, E. Real, L. Gardner, Description of stress-strain curves for stainless steel alloys, *Materials and Design*. 87 (2015) 540–552.
- [27] M. Ashraf, L. Gardner, D. A. Nethercot, Strength enhancement of the corner regions of stainless steel cross-sections, *Journal of Constructional Steel Research*. 61 (1) (2005) 37–52.
- [28] R. B. Cruise, L. Gardner, Strength enhancements induced during cold forming of stainless steel sections, *Journal of Constructional Steel Research*. 64 (11) (2008) 1310–1316.
- [29] P. Keerthan, M. Mahendran, New design rules for the shear strength of LiteSteel beams, *Journal of Constructional Steel Research*. 67 (6) (2011) 1050–1063.
- [30] B. W. Schafer, T. Peköz, Computational modeling of cold-formed steel: Characterizing geometric imperfections and residual stresses, *Journal of Constructional Steel Research*. 47 (3) (1998) 193–210.
- [31] ABAQUS 6.14 Analysis User's Guide Volume II: Analysis, Dassault Systèmes, Rhode Island, USA, 2014.
- [32] R. G. Dawson, A. C. Walker, Post-buckling of geometrically imperfect plates, *Journal of the Structural Division*. 98 (1) (1972) 75–94.
- [33] L. Gardner, D. A. Nethercot, Numerical Modeling of Stainless Steel Structural Components – A Consistent Approach, *Journal of Structural Engineering*. 130 (10) (2004) 1586–1601.
- [34] M. Theofanous, L. Gardner, Experimental and numerical studies of lean duplex stainless steel beams, *Journal of Constructional Steel Research*. 66 (6) (2010) 816–825.
- [35] N. Saliba, L. Gardner, Experimental study of the shear response of lean duplex stainless steel plate girders, *Engineering Structures*. 46 (2013) 375–391.

- [36] O. Zhao, L. Gardner, B. Young, Buckling of ferritic stainless steel members under combined axial compression and bending, *Journal of Constructional Steel Research*. 117 (2016) 35–48.
- [37] EN1993-1-1. Eurocode 3 – Design of steel structures – Part 1 – 1: General rules and rules for buildings, European Committee for Standardization (CEN), Brussels, 2005.
- [38] B. Schafer, T. Pekoz, Direct strength prediction of cold-formed steel members using numerical elastic buckling solutions, *Proceedings of the fourteenth international speciality conference on cold-formed steel structures*, University of Missouri-Rolla, Missouri, USA, 1998, 69-76.
- [39] B. W. Schafer, Review: The Direct Strength Method of cold-formed steel member design, *Journal of Constructional Steel Research*. 64 (2008) 766–778.
- [40] C. H. Pham, G. J. Hancock, Direct strength design of cold-formed C-sections for shear and combined actions, *Journal of Structural Engineering*. 138 (6) (2012) 759–768.
- [41] AISI-S100-2007. North American specification for the design of cold-formed steel structural members, American Iron and Steel Institute (AISI), Washington (DC), USA, 2007.